JOURNAL OF SPACECRAFT AND ROCKETS
Vol. 34, No. 4, July–August 1997

Fin Leading-Edge Sweep Effect on Shock–Shock Interaction at Mach 6

Scott A. Berry* and Robert J. Nowak†
NASA Langley Research Center, Hampton, Virginia 23681-0001

The effects of fin leading-edge sweep on peak heating rates due to shock–shock interaction have been experimentally examined in the NASA Langley Research Center 20-Inch Mach 6 Tunnel. The shock interaction was produced by the intersection of a planar incident shock (16.8-deg shock angle relative to the freestream, generated by a 9-deg wedge) with the bow shock formed around a 0.5-in.-diam cylindrical leading-edge fin. Heating distributions along the leading-edge stagnation line have been obtained using densely spaced thin-film resistive-type sensors. Schlieren images were obtained to illustrate the very complex shock–shock interactions. The fin leading-edge sweep angle was varied from 15 deg swept back (relative to the normal to the freestream) to 45 deg swept forward for a freestream unit Reynolds number of 2×10^6/ft. Two models were utilized during the study, one with 0.025-in. spacing between gauge centers, and the other with 0.015-in. spacing. Gauge spatial resolution on the order of 0.015 in. appeared to capture the narrow heating spike accurately. Peak heating due to shock interaction was maximized when the fin was swept forward 15 and 25 deg, both promoting augmentations over seven times the baseline value. The schlieren images for these cases revealed Type IV and Type III interactions, respectively.

Nomenclature

Ch = nondimensional Stanton number, $q/\rho_\infty u_\infty (h_{t2} - h_\infty)$
Ch_{ref} = reference Stanton number, measured for each run from undisturbed end of model
h_{t2} = stagnation enthalpy behind normal shock, Btu/lbm
h_∞ = freestream enthalpy, Btu/lbm
L = length of leading edge, 4 in.
M_∞ = freestream Mach number
P_{t1} = stagnation pressure, psi
q = heat transfer rate, Btu/ft$^2 \cdot$ s
Re_∞/ft = freestream unit Reynolds number, ft^{-1}
T_{t1} = stagnation temperature, °R
T_∞ = freestream temperature, °R
t = time, s
u_∞ = freestream velocity, ft/s
x = distance measured from incident shock location, in.
β = incident shock angle relative to the freestream, deg
δ = shock generator angle relative to the freestream, deg
λ = fin sweep angle relative to the normal to the freestream (where positive is defined as swept back and negative as swept forward), deg
ρ_∞ = freestream density, slug/ft^3

Introduction

HYPERSONIC flight vehicles are characterized by shock wave systems that, in general, lie close to the body and often generate highly complex two- and three-dimensional shock–shock interaction regions with potentially high heating levels on surfaces near the interaction. This was clearly evident on the first manned hypersonic test vehicle, the X-15, where on a flight in which a ramjet test article was attached to the ventral fin, structural damage to the engine pylon occurred as a result of shock impingement and the test article was lost in flight. Designers of subsequent hypersonic flight vehicles, such as the Shuttle Orbiter, have, at some point in the design process, had to consider the possible ramifications of shock interactions on the aerothermal loads to the vehicle. The effect of shock interactions is especially important in the design of future hypersonic air-breathing cruise vehicles such as the (now canceled) National Aerospace Plane (NASP) (see Fig. 1), where the leading edges of the scramjet inlet will have to be designed to endure sustained and augmented heat loads.

Edney[1] described the six basic interaction types (see Fig. 2). Of the six, the Type IV interaction has generally been identified as the case with the highest heating augmentation, because a highly energized supersonic jet is produced that can directly impinge on the surface. Heating level augmentations of over an order of magnitude higher than stagnation-point heating values have been reported in recent shock interaction studies.[2] A vast majority of the most recent studies, however, have dealt with the two-dimensional interaction, typified by the so-called shock-on-cowl work initiated in support of the NASP program. The two-dimensional interaction is generated by a planar bow or compression shock intersecting a shock formed around the engine cowl leading edge, which is parallel to the plane of the incident shock. As a consequence of the NASP program, the two-dimensional interaction has been extensively examined through a series of experimental and computational studies (see, for example, Refs. 2–6). These recent studies have provided, among other things, an increased understanding of the details of the interactions and an appreciation for the instrumentation spatial density required to accurately define the heating peak and distribution.

Contrary to the recent experimental and computational efforts conducted on the two-dimensional interaction, the three-dimensional shock-on-fin interaction has not been as extensively examined. The three-dimensional interaction is typically generated by the intersection of a planar incident shock with a shock formed by a wing or strut leading edge, which is in a plane perpendicular to the incident shock. Early three-dimensional experiments[7–10] were focused on the problem of shock interaction on swept-back wings, struts, or fins. At the time, there were few applications that required swept-forward leading edges; as a consequence, these studies did not address the forward sweep cases where the potential is strongest for a Type IV interaction to generate a supersonic jet that impinges normal to the surface. The heating distribution associated with this strong Type IV would require very closely spaced instrumentation to accurately measure the strong and narrow peak. For current applications, such as the internal surfaces of scramjet engines, swept-forward leading edges (relative to the incident shock) and strong Type IV interactions are possible. Thus, for conditions where the Type IV interaction heating would be maximized, an

Presented as Paper 96-0230 at the AIAA 34th Aerospace Sciences Meeting, Reno, NV, Jan. 15–18, 1996; received Feb. 29, 1996; revision received March 10, 1997; accepted for publication March 15, 1997.

*Research Engineer, Aerothermodynamics Branch.
†Research Engineer, Aerothermodynamics Branch. Member AIAA.

Table 1 Nominal flow conditions for 20-Inch Mach 6 Tunnel

M_∞	Re_∞/ft	P_{t1}, psi	T_{t1}, °R	ρ_∞, 10^{-4} slug/ft^3	T_∞, °R	μ_∞, ft/s
5.84	0.5	30	869	0.17	111	3019
5.96 (±2%)	2.2 (±5%)	127 (±2%)	913 (±1%)	0.62 (±8%)	113 (±4%)	3100 (±0.5%)
5.98	4.0	260	935	1.23	114	3139
6.02	8.0	475	935	2.18	113	3142

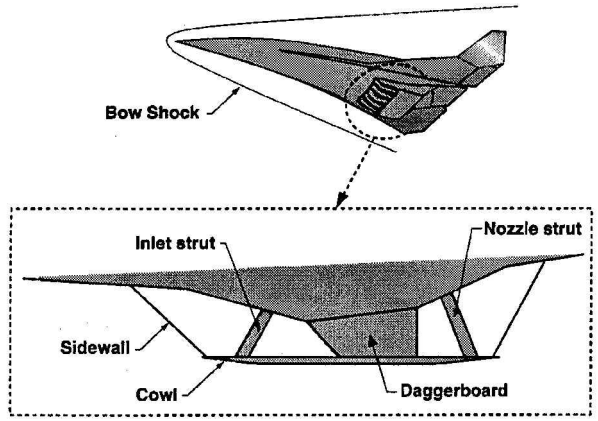

Fig. 1 Shock interaction regions for a hypersonic air-breathing cruise vehicle.

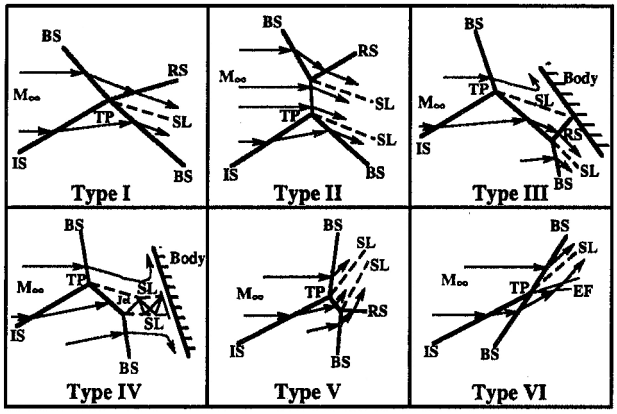

Fig. 2 Shock interaction types as classified by Edney[1]: IS = incident shock, BS = bow shock, RS = reflected shock, EF = expansion fan, TP = triple point, and SL = shear layer.

experimental dataset was not available for comparison with recent three-dimensional computational efforts detailed in Refs. 11 and 12.

The current study systematically examines the effect of fin leading-edge sweep on the shock–shock interaction process at Mach 6. A highly instrumented cylindrical leading edge fin, 0.5-in. diam, which could be placed at arbitrary fin sweep angles λ between ±45 deg, was subjected to a planar shock generated with a two-dimensional sharp-leading-edge wedge. Detailed heating distributions along the stagnation line of the cylinders were measured with thin-film resistance gauges. These measurements were complemented with high-quality schlieren photography. The purpose of this paper is to present these initial results that detail the effect of fin sweep angle on three-dimensional shock interactions for the fixed conditions of 0.5-in.-diam leading edge, 16.8-deg incident shock angle, freestream Mach number 6, and freestream unit Reynolds number 2×10^6/ft. Also presented are qualitative results in the form of schlieren images obtained over a range of Reynolds numbers for zero and 20-deg swept-forward fin sweep angles. The current experimental results provide a better understanding of the complex nature of three-dimensional interactions and are applicable for future three-dimensional shock interaction code calibration efforts.

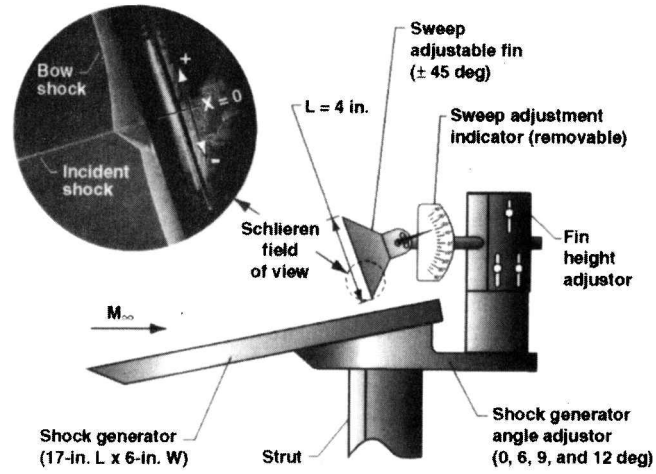

Fig. 3 Sketch of experimental setup.

Experimental Methods

Facility

The experiment was conducted in the 20-Inch Mach 6 Tunnel at the NASA Langley Research Center. A detailed description of this hypersonic blowdown facility, which uses heated, dried, and filtered air as the test gas, is provided in Ref. 13, along with performance characteristics. Typical operating conditions for the tunnel are stagnation pressures ranging from 30 to 500 psia, stagnation temperatures from 760 to 1000°R, and freestream unit Reynolds numbers from 0.5 to 9×10^6/ft. The facility has a bottom-mounted model injection system that can insert models from a sheltered position to the tunnel centerline in less than 1.0 s. As discussed in Ref. 14, 256 channels of signal conditioning are available for thin-film instrumentation and are interfaced to a 16-bit analog-to-digital data acquisition system, which typically interrogates each channel at a rate of 50 samples/s.

For a majority of the current study, both heating measurements and schlieren images were acquired on the 0.025-in.-spacing thin-film baseline model at a freestream unit Reynolds number of 2×10^6/ft. A few of the fin sweep cases were repeated with the 0.015-in.-spacing model. A limited number of schlieren-only runs were acquired over a range of freestream unit Reynolds number of 0.5–8×10^6/ft. Table 1 presents the nominal flow conditions for these cases, as well as the statistical repeatability of the flow conditions as determined from all of the runs made at a freestream unit Reynolds number of 2×10^6/ft.

Models

The experimental setup (sketched in Fig. 3) consists primarily of a sharp-leading-edge, two-dimensional, flat-plate shock generator and a cylindrical-leading-edge fin that is instrumented with densely spaced thin-film gauges. The uninstrumented stainless-steel shock generator is 6 in. wide by 17 in. long; it was set at an angle δ of 9 deg and produces an incident shock angle β of 16.8 deg. The sweep-adjustable fin was held above the shock generator to place the fin root out of the boundary layer on the shock generator plate and to isolate the shock–shock interaction from the shock–boundary-layer interaction. The fin leading edge consisted of a 4-in.-long instrumented Macor® (a machinable glass ceramic) cylindrical rod with a diameter of 0.5 in. (Macor is a trademark of Corning Glass Works.) Two highly instrumented cylinders, with the thin-film gauges spaced along the leading-edge stagnation line, were available for this study

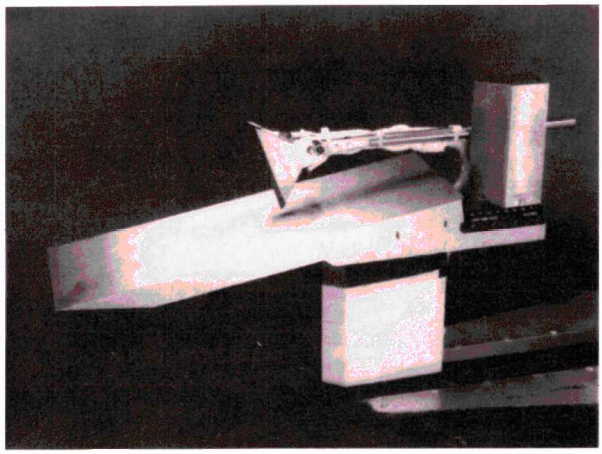

Fig. 4 Photograph of model installed in NASA Langley Research Center 20-Inch Mach-6 Tunnel.

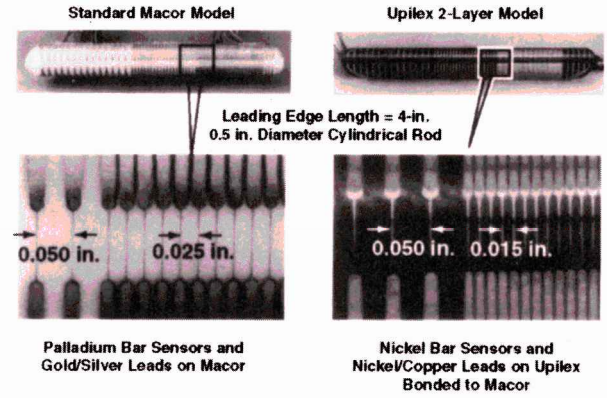

Fig. 5 Details of thin-film instrumentation.

and will be described in the following sections. The fin can be adjusted for fin leading-edge sweep angles λ of ± 45 deg with repeatable accuracy of better than 0.5 deg. As can be seen in the sketch, a removable sweep adjustment indicator was provided to assist in the accurate setting of the fin sweep angle prior to a run and was verified with an inclinometer. A photograph of the model installed in the 20-Inch Mach 6 Tunnel is shown in Fig. 4.

Instrumentation

For the present study, emphasis was placed on the development of thin-film instrumented models, which provided an improvement in gauge resolution over previous three-dimensional shock interaction studies. Standard mechanical deposition techniques (such as vapor deposition or sputtering) have been used at NASA Langley Research Center to produce high-quality thin-film resistive gauges.[15] However, the best resolution that was obtainable using these techniques on a cylindrical Macor rod was 0.025-in. spacing between gauge centers. The gauges for this baseline model were mechanically deposited using vapor deposition. The limiting factor for fabrication of this model was the ability to accurately maintain the clearance between the sensor leads on the cylindrical surface. With standard mechanical deposition techniques, line-of-sight apparatuses are generally used during the fabrication process, which has difficulty placing high-quality, tightly packed gauges and leads on curved surfaces.

While standard techniques were used to provide a baseline model, new approaches were also examined to improve the leading-edge spatial resolution. One of the more promising approaches involved the use of a thin polyimide film as a transfer medium to place high-quality gauges down on a curved surface. The thin-film gauges were etched onto a flat polyimide film, and the film was later wrapped and bonded to the cylindrical rod. Using this technique, the resolution was improved to 0.015-in. spacing between gauges. (With this technique, it is possible to deposit sensors whose spacing is 0.005 in. As the widths of sensor leads are typically greater than 0.005 in., the difficulty becomes one of packaging the leads away from the sensors.) The polyimide film that was chosen during the development process was a 50-μm (0.002-in.) thick type S Upilex® film because its excellent surface quality allowed for high-quality gauges. (Upilex is a registered trademark of Ube Industries, Ltd.)

Thus two instrumented models were available during this study: the baseline standard Macor model, which had a total of 80 gauges with a resolution of 0.025 in. over a 1-in. section near where the shock interaction occurred, and the new Upilex model, which had a total of 108 gauges with a resolution of 0.015 in. On both models, the spacing requirements were relaxed for the remainder of the 4-in. leading edge, with regions where the gauge spacing was 0.050 and 0.100 in. Photographs of the instrumented cylinders used in this study are presented in Fig. 5. The Macor model has 0.002×0.100-in. palladium sensors that are connected to a combination of gold and silver leads. The Upilex model has 0.002×0.100-in. nickel sensors that are connected to a combination of nickel and copper leads.

To provide details of the shock interaction process, a single-pass, magnifying-lens schlieren system was set up to zoom in and capture a 2-in.-diam area centered around the interaction point (see Fig. 3). A xenon light source was used, providing a flash duration of approximately 1–2 μs. The images were recorded on 4×5-in. black-and-white film and on 30-frame/s video. The model was front-lighted to illuminate the gauges on the picture for a scale reference.

Data Reduction and Uncertainty

Calibrations, in a uniform-temperature oil bath, over a temperature range of 75–425°F, were performed on both models. The resistivity of palladium is reported to be essentially linear over this temperature range, and this was confirmed by the calibrations. A linear fit to the variation of resistance with temperature allows for an uncertainty on the order of 3%, which is similar to previous thin-film studies.[15,16] However, for the Upilex model, nickel was chosen as the sensor material (mainly due to its high-temperature sensitivity), and it has a more nonlinear response to changes in temperature. Thus, a second-order curve fit was used for the Upilex model to convert the millivolt output of the gauges to temperature, which typically provided better than 1% uncertainty.

Data reduction was performed using a newly developed one-dimensional heat conduction code,[17] which incorporates both an analytical and a numerical (finite volume) heat transfer scheme. The analytical solution, the classic Cook–Felderman technique,[18] is developed from heat conduction theory for a one-dimensional, semi-infinite solid, assuming constant thermal properties of the substrate. An empirically derived correction factor is used to allow for the effects of variable thermal properties. A previous comparison of this analytical technique with the finite volume technique has shown excellent agreement ($\approx$1–2% error) (Ref. 19). Thus, the baseline Macor model was analyzed using the analytical technique. The finite volume technique takes direct account of the variable substrate thermal properties and removes the restriction of a semi-infinite substrate (thus allowing for a multiple layer analysis). This was an important consideration for the Upilex model because for the test times associated with conventional hypersonic facilities, the thermal penetration depth of the heat pulse will exceed the thickness of the polyimide film and invalidate the semi-infinite assumption. Thus, for the Upilex model the heat transfer was computed using the finite volume technique, with 5 points in the Upilex layer and 244 points in the Macor sublayer. Recent updates to the thermal properties of both Macor and Upilex have been included in the code and are discussed in Ref. 17. The current analysis of the Upilex model data has been conducted with the assumption that the approximately 0.001-in. bondline is thermally invisible. Reliable thermal property information for the high-temperature epoxy used was not available. Thermal property analysis of the bonding material, as well as further analysis of the polyimide film, is ongoing.

The individual thin-film resistance sensors provided temperature–time histories that were integrated to compute the heating rate and normalized to provide Stanton numbers Ch. Primary contributions to the uncertainty in the heat-transfer results include the

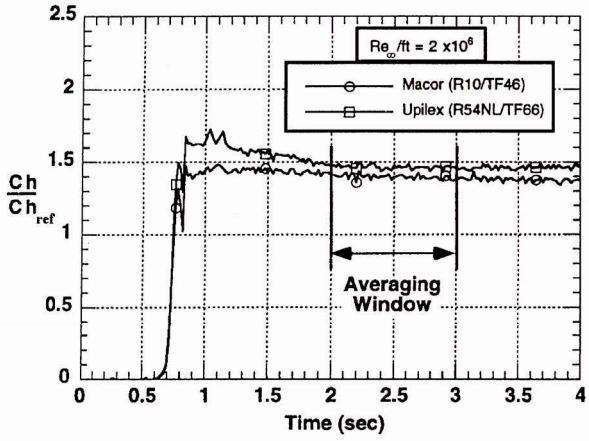

Fig. 6 Comparison of normalized heating time histories for peak-heating gauges, between the two models, for the shock-on-fin case of zero sweep.

uncertainties associated with the thermal properties of the substrate material (including the neglected bond layer) and possible lateral conduction effects due to the strong heating gradient in the vicinity of the interaction. The baseline model, with construction, calibration, and data acquisition and reduction similar to previous studies,[14–16,19,20] is believed to be accurate to within 8–10% in the regions beyond the influence of the shock interaction. As a strong temperature gradient exists where the shock interaction impinges on the surface, lateral conduction within the model must be taken into account in order to confine the uncertainty levels to the acceptable 8–10% range. A preliminary one-dimensional analysis of conduction (in the lateral direction) due to the measured temperature gradient along the attachment line indicates that a one-dimensional analysis (in the normal direction) significantly underpredicts the peak heating values (on the order of 30–40%). An accurate estimate of the error would require a three-dimensional conduction capability that is not currently available. As the lateral conduction is driven by the surface temperature gradient, one method to reduce the error is to analyze the data at the earliest possible time after flow is fully established, when the surface temperature rise (and thus the gradient) is the smallest. Unfortunately, for the current dataset the model is not yet fully injected when the flow establishes at roughly $t = 0.85$ s, and thus the flow is only quasisteady, i.e., the peak fluctuates between different gauges, until the model stops at the tunnel centerline at $t = 2$ s. The roughly 1-s exposure to quasisteady flow allows a significant temperature gradient to build up, and thus leads to the large conduction error. (Note that the instantaneous heating rate at $t = 0.85$ s is on the order of 30% higher than the results obtained when the data is analyzed at $t = 2$ s.) The uncertainty levels for the Upilex model should be slightly higher than for the baseline model, as the thermal properties of the Upilex layer and the bond line are not accurately known. However, the conduction errors should be less, as Upilex is a much better insulator than Macor.

To minimize the uncertainty associated with the thermal properties on the comparisons between the two models, the Stanton number calculated for each gauge was normalized by the calculated Stanton number for an average of gauges that were on the undisturbed portion of the cylinder during each run. A comparison, between the two models, of the normalized Stanton number histories for the peak heating gauges for the case of shock impingement with fin sweep of zero is shown in Fig. 6. Time $t = 0$ corresponds to the start of injection, and at $t = 2$ the model has stopped at the tunnel centerline. The Stanton number remains constant with time once the model reaches the centerline, and consequently the distributions shown in the following section are based on time-averaged data for a 1-s interval starting at $t = 2$. Within this averaging window the normalized Stanton number for the Upilex model is 3–4% higher than the baseline results: this may be due in part to the neglected bond line. Smaller averaging windows were examined, with minimal effect on the overall distribution or peak.

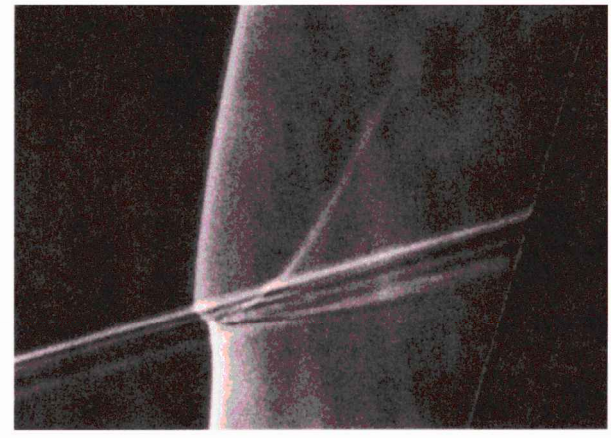

a) Schlieren image

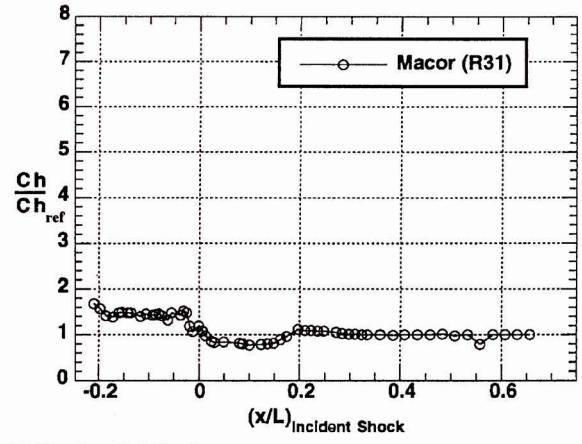

b) Heating distribution

Fig. 7 Results for $\lambda = 15$ deg.

Results and Discussion

Heat-transfer measurements and schlieren images were obtained for a range of fin sweep angles that varied between $\lambda = +15$ deg and $\lambda = -45$ deg for a freestream unit Reynolds number of 2×10^6/ft. The results presented in Figs. 7–15 are for a roughly 5-deg increment. A finer increment in fin sweep angles was obtained, and these results are included in the summary peak heating plot in Fig. 16. The images were used to identify the location of the extrapolated position of the incident shock, as shown in the labeled schlieren image that was included in the sketch in Fig. 3. The planar incident shock is wider than the fin bow shock. As conventional schlieren systems integrate across the entire light path, the incident shock appears in the image to continue through the initial triple point, thereby locating the exact gauge number of the $x = 0$ location. On transferring x/L to the incident shock location, the heating distributions collapse on top of each other even though the actual location of the impingement may differ run to run. As will be shown in the subsequent heat transfer distributions, excellent agreement was found in the overall trends between different runs in which both the location of the model and the model type were varied. Note that, in some of the close-up schlieren images, unusually thick incident shocks occur. This nonplanar shock condition appears to be attributable to defects to the leading-edge corners of the shock generator, which resulted from handling.

Fin Sweep of 15 deg

The flow-visualization and heating results for $\lambda = +15$ deg are presented in Fig. 7. The schlieren image (Fig. 7a) reveals an interaction (perhaps a Type V) that produces a very small transmitted shock that remains close to the triple point. The resulting shear layer is turned up at an angle such that reattachment occurs quite some distance above the extrapolated position of the incident shock. This

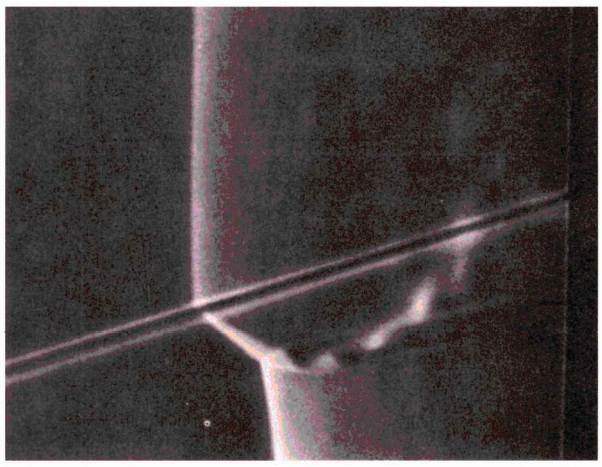

a) Schlieren image

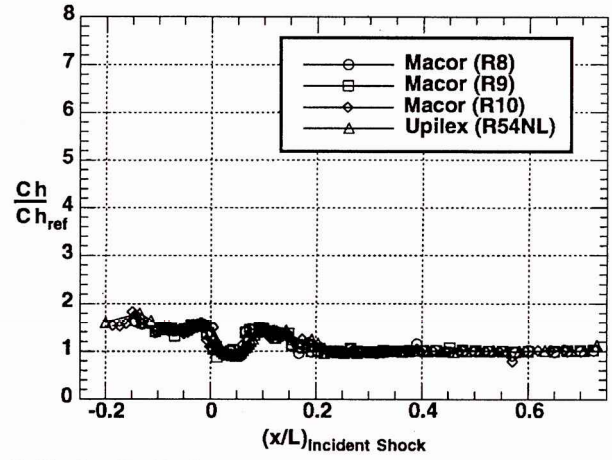

b) Heating distribution

Fig. 8 Results for $\lambda = 0$ deg.

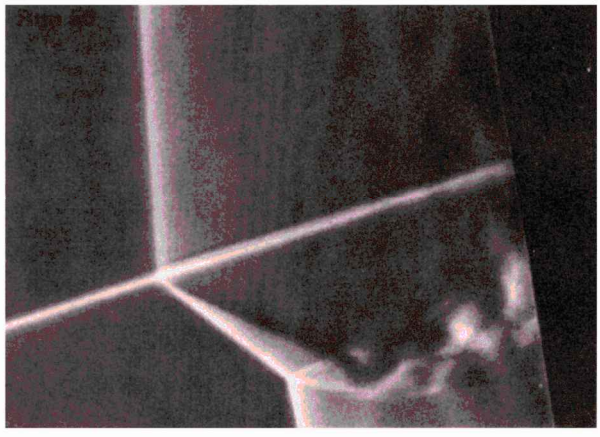

a) Schlieren image

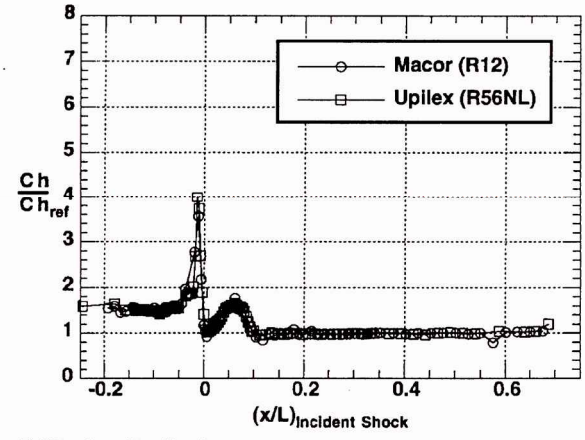

b) Heating distribution

Fig. 9 Results for $\lambda = -10$ deg.

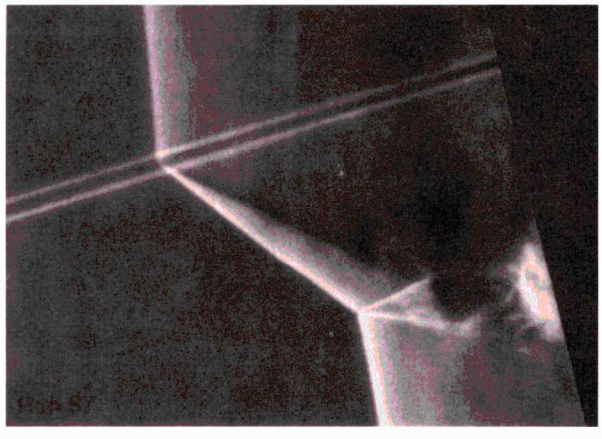

a) Schlieren image

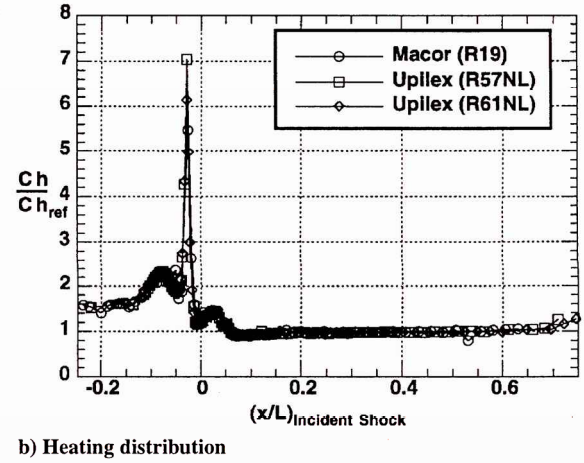

b) Heating distribution

Fig. 10 Results for $\lambda = -15$ deg.

is consistent with the heating results (Fig. 7b), which reveal that, in general, the overall heating levels are quite low (at most 1.5 times the undisturbed value) and that reattachment occurs midway up on the leading edge (at $x/L \approx 0.2$).

Zero Fin Sweep

Figure 8 shows the results for $\lambda = 0$ deg (the leading edge is perpendicular to the freestream). The schlieren results (Fig. 8a) reveal that a glancing Type IV interaction has been set up where the supersonic jet bends up and away from the fin leading edge. The shear-layer or jet impingement region appears to be closer to (but still above) the incident shock location than in the preceding example. The heating results in Fig. 8b confirm this and also show that the heating augmentation due to shear-layer impingement is increasing.

Fin Sweep of −10 deg

The results for $\lambda = -10$ deg are presented in Fig. 9. The schlieren photograph reveals that the transmitted shock length has increased slightly and that the shear layer now impinges below the $x/L = 0$

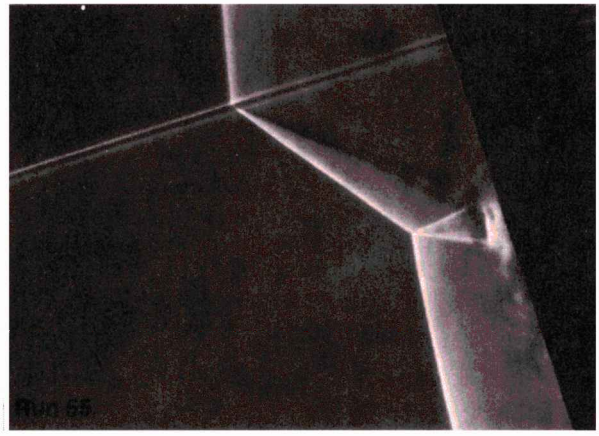

a) Schlieren image

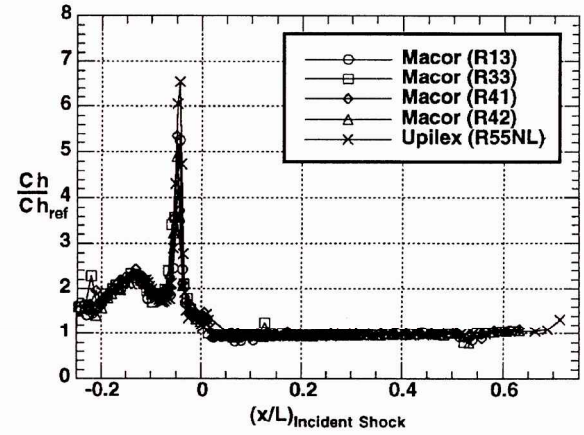

b) Heating distribution

Fig. 11 Results for $\lambda = -20$ deg.

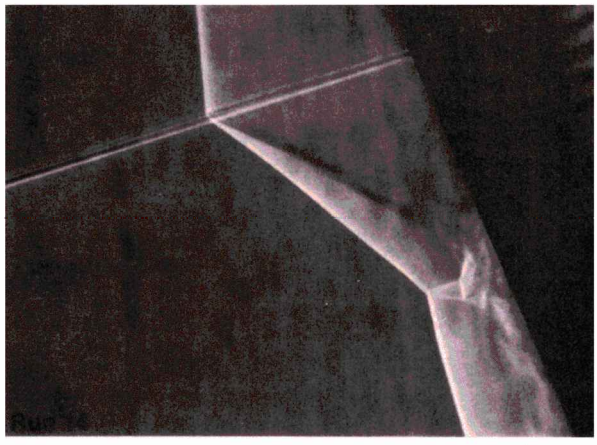

a) Schlieren image

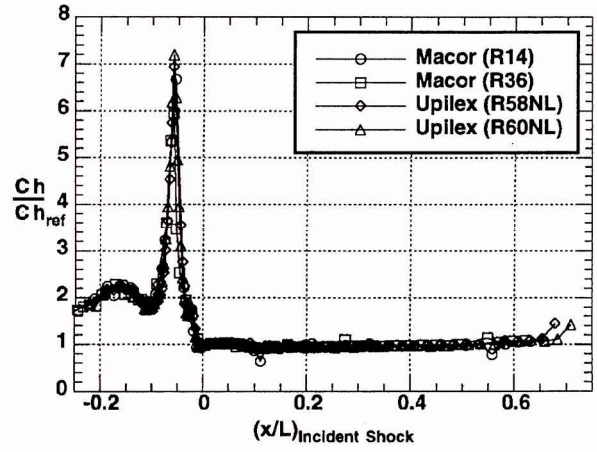

b) Heating distribution

Fig. 12 Results for $\lambda = -25$ deg.

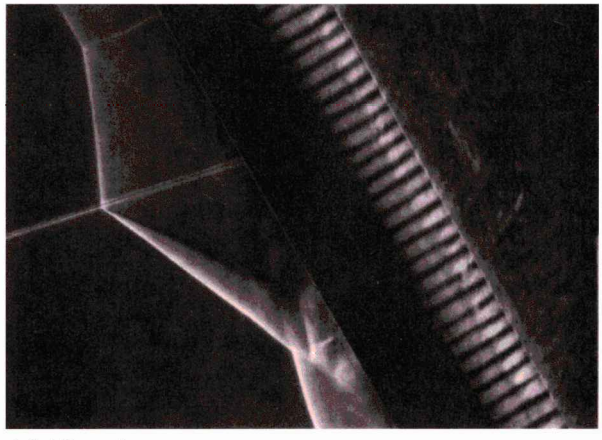

a) Schlieren image

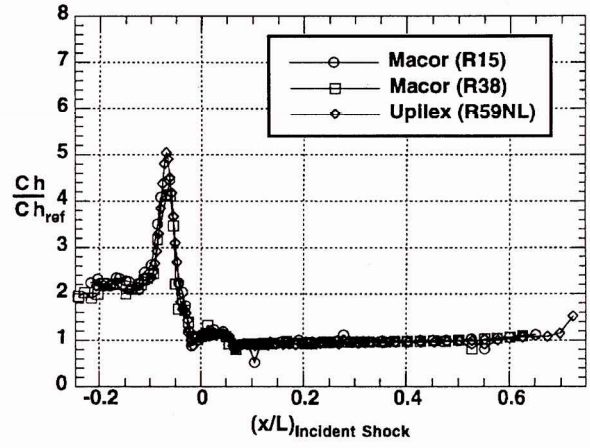

b) Heating distribution

Fig. 13 Results for $\lambda = -30$ deg.

location, resulting in a more classic Type IV interaction. There appears to be a slight upward inclination of the terminating jet, however. The heating results reveal that indeed a strong and narrow peak has emerged with a peak value of heating a little over four times the baseline value.

Fin Sweep of −15 deg

Figure 10 presents the results for $\lambda = -15$ deg. The fin is now nearly perpendicular to the incident shock. The transmitted shock length has increased, and the supersonic jet of this Type IV interaction now terminates directly into the fin leading edge just below the incident shock location. The heating results reveal a strong and narrow peak with minor secondary peaks on either side. The peak heating value is on the order of seven times the baseline value. Although not visible in Fig. 10a, the leads can be traced forward to show that, for the 0.015-in. spacing model, the supersonic jet width is approximately the distance between three of the gauges (≈0.030 in.).

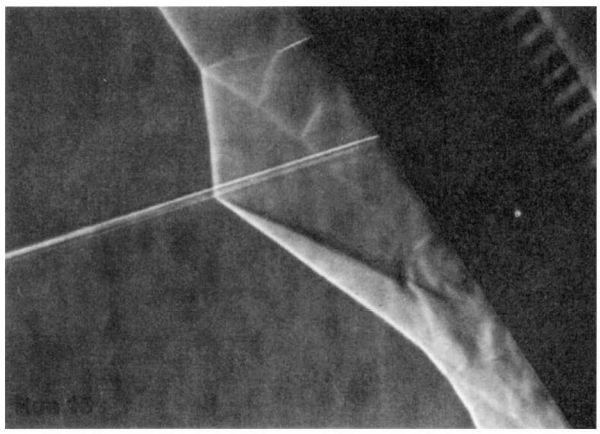

a) Schlieren image

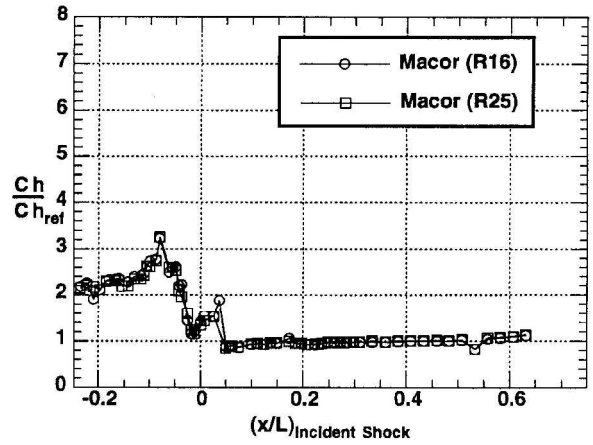

b) Heating distribution

Fig. 14 Results for $\lambda = -35$ deg.

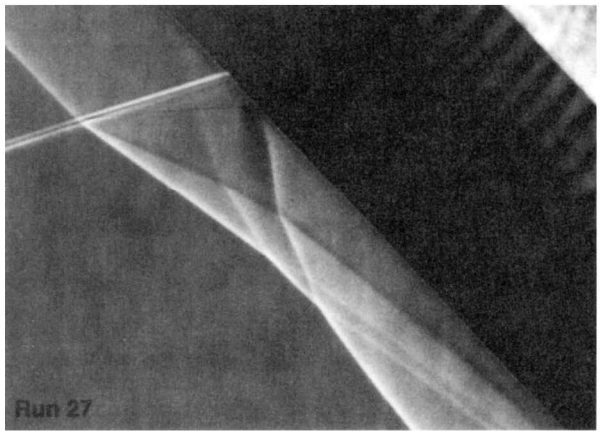

a) Schlieren image

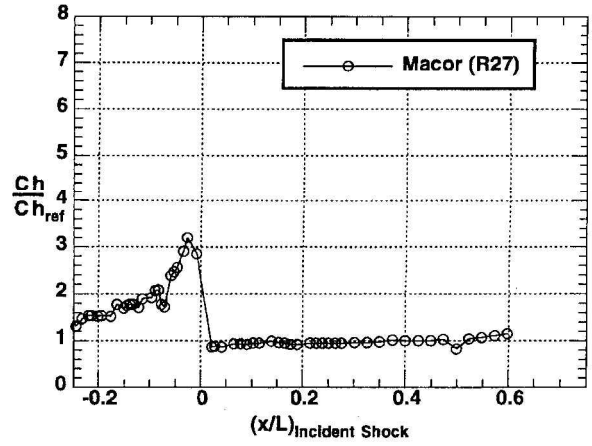

b) Heating distribution

Fig. 15 Results for $\lambda = -45$ deg.

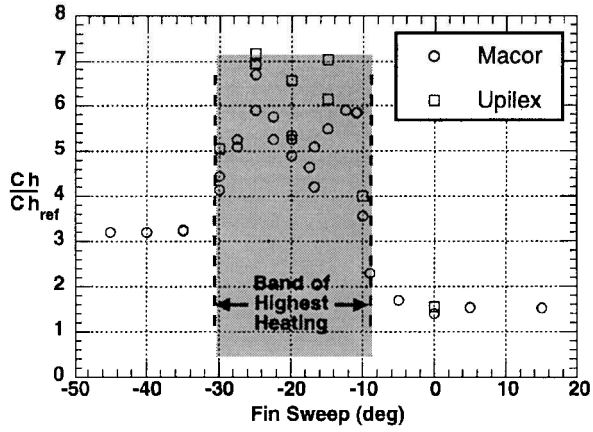

Fig. 16 Normalized peak heating values as a function of fin sweep angles.

Fin Sweep of −20 deg

The results for $\lambda = -20$ deg are presented in Fig. 11. The schlieren image shows that the transmitted shock has become quite long and that the shear layer has begun to impinge directly on the fin leading edge without further processing by the supersonic jet shock system. The heating results show a slight reduction in the overall peak heating value as well as a slight broadening of the high heating zone.

Fin Sweep of −25 deg

The results for $\lambda = -25$ deg are presented in Fig. 12. The schlieren results reveal that the interaction is becoming more like a Type III interaction, where the shear layer emerging from the first triple point dominates the surface impingement process. This is verified by the heating results, as the peak heating location corresponds to the thin-film gauge directly in line with the shear layer in the schlieren photograph for all four runs. The overall peak heating level is again around seven times the baseline value, and the peak width has broadened significantly.

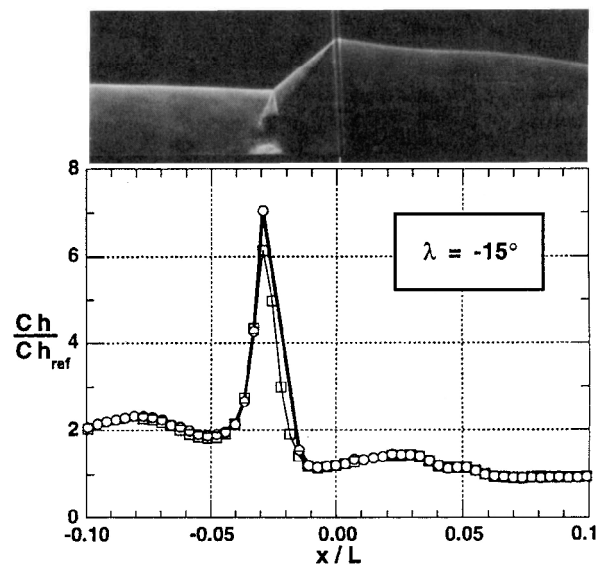

Fig. 17 Shock interaction flowfield at location of peak heating for $\lambda = -15$ deg.

Fin Sweep of −30 deg

Figure 13 presents the results for $\lambda = -30$ deg. The interaction is beginning to resemble a Type II interaction, although the shear layer emanating from the initial triple point still appears to dominate the surface impingement process. The heating results confirm this as a strong peak (with overall peak heating level of five times the baseline value) that coincides with the thin-film gauges directly under the shear layer impingement. The width of the main peak is quite broad, and a minor secondary peak is evident, which may correspond to the reattachment of the shear layer emanating from the secondary triple point.

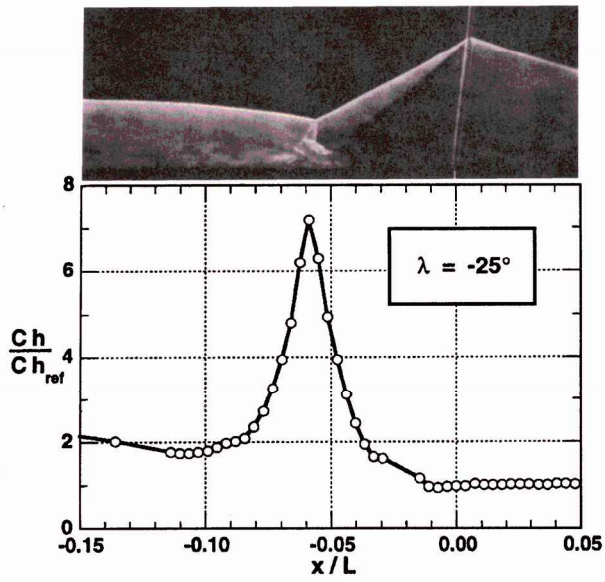

Fig. 18 Shock interaction flowfield at location of peak heating for $\lambda = -25$ deg.

Fin Sweep of −35 deg

The results for $\lambda = -35$ deg are presented in Fig. 14. The schlieren image reveals a Type II interaction that appears to support a complex merging of the shear layers associated with the two different triple points. The heating results reveal a continued breakdown of the primary peak as well as strengthening of the secondary peak. The overall peak heating level has dropped to just over three times the baseline value.

Fin Sweep of −45 deg

Figure 15 presents the results for $\lambda = -45$ deg. A Type I interaction has emerged that involves a complex pattern of crossing shock and shear layers. The heating results show that the peak heating location corresponds to the initial impingement point just below the extrapolated incident shock location. The overall peak heating augmentation is just over 3.

Peak Heating Due to Fin Sweep

Figure 16 presents the results on the peak heating as a function of fin leading-edge sweep angle for all the runs. Many of the repeat runs were acquired to better locate the shock impingement heating peaks in the vicinity of high-spatial-resolution gauges. Thus, some of the scatter shown in Fig. 16 is due to lower-resolution gauges missing the heating peaks. The Upilex model shows approximately a 15–20% overall increase in peak heating level, which is believed to be partially attributable to the increased spatial resolution of the Upilex model. A double-humped trend is evident within the band of highest heating ($\lambda = -10$ to -30 deg), with peaks for both $\lambda = -15$ and -25 deg. The $\lambda = -15$-deg case corresponds to a Type IV interaction where the heating augmentation is due to the direct impingement of the supersonic jet as shown in the correctly aligned composite heating–schlieren image of Fig. 17. The $\lambda = -25$-deg

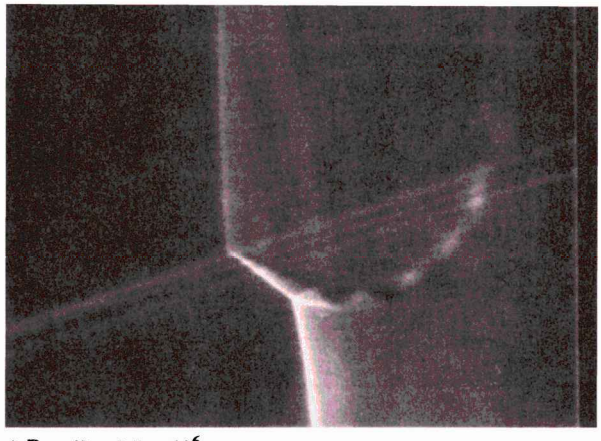

a) Re_∞/ft = 0.5 × 10^6

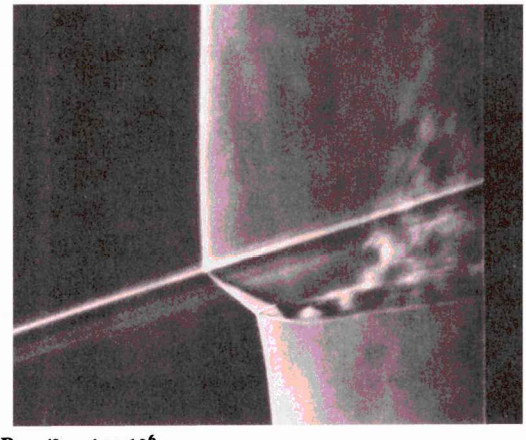

c) Re_∞/ft = 4 × 10^6

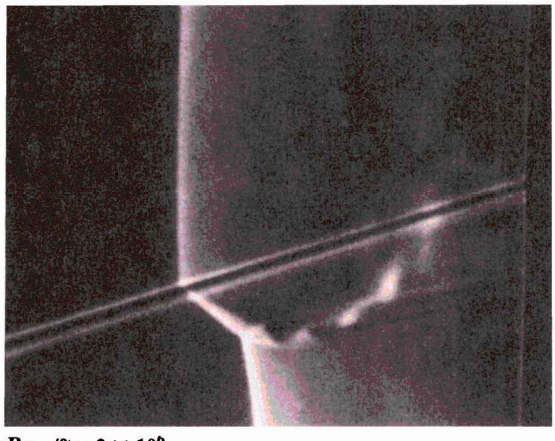

b) Re_∞/ft = 2 × 10^6

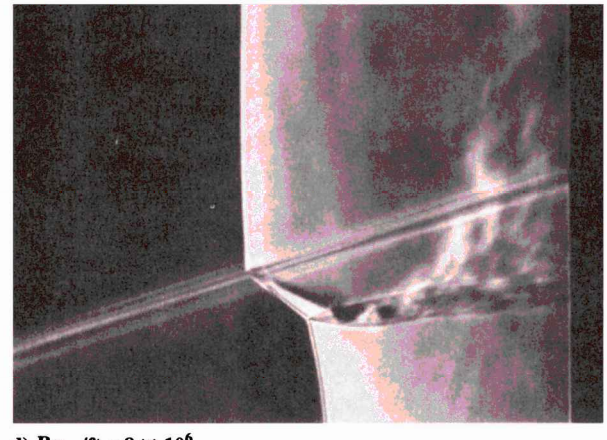

d) Re_∞/ft = 8 × 10^6

Fig. 19 Effect of Reynolds number on shock interaction for $\lambda = 0$ deg.

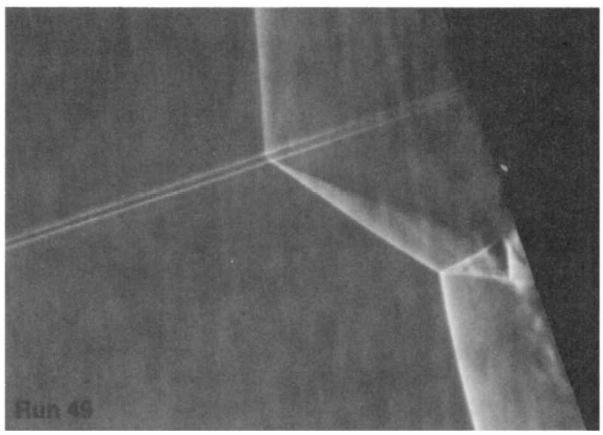

a) Re_∞/ft = 0.5 × 10^6

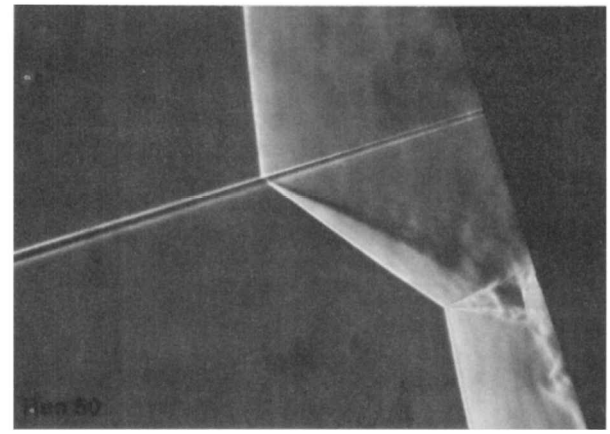

c) Re_∞/ft = 4 × 10^6

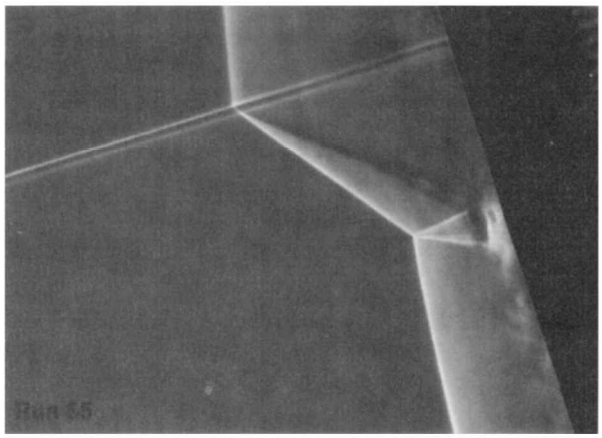

b) Re_∞/ft = 2 × 10^6

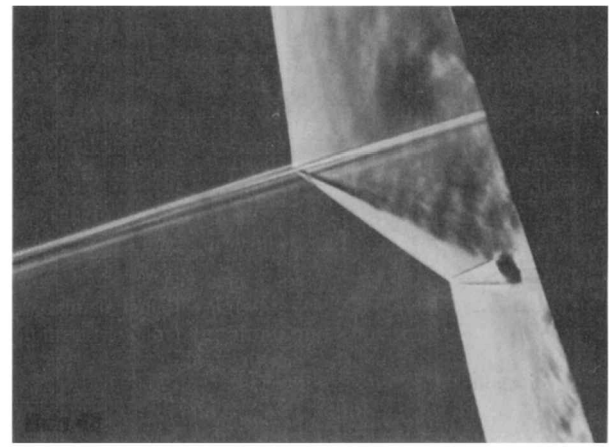

d) Re_∞/ft = 8 × 10^6

Fig. 20 Effect of Reynolds number on shock interaction for $\lambda = -20$ deg.

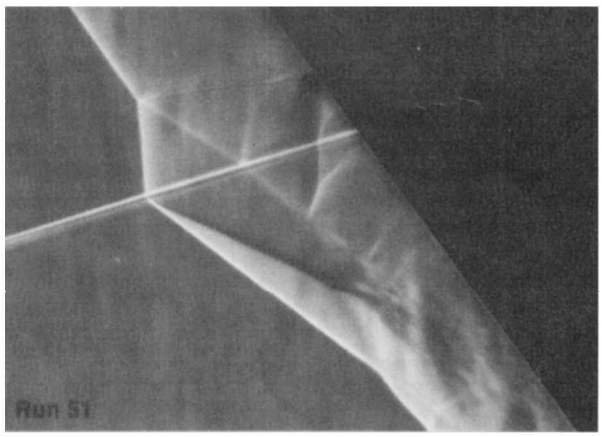

a) $\lambda = -38$ deg

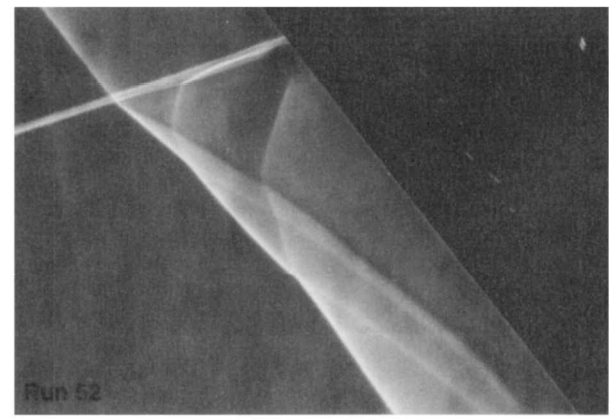

b) $\lambda = -39$ deg

Fig. 21 Effect of small fin-sweep angle change at Re_∞/ft = 2×10^6/ft.

case corresponds to a Type III interaction where the heating augmentation is due to the shear-layer impingement as shown in Fig 18.

Reynolds Number Effects

Although the heat-transfer results were for a single freestream unit Reynolds number, a limited number of schlieren only runs were obtained over the Reynolds number range of 0.5–8.0 ×10^6/ft. Figure 19 presents the results for this Reynolds number range for the case of zero sweep. Figure 20 presents the results for this same range for $\lambda = -20$ deg. In both cases, the shear layer or jet emanating from the triple point appears to break up and become more diffuse as the Reynolds number increases (perhaps an indicator of unsteadiness associated with transition and turbulence). Also noteworthy are the large-scale vortices that form along the surface for $\lambda = -20$ deg, particularly evident in Figs. 20b and 20d.

Small Fin Sweep Increments

An example of the extreme sensitivity of shock interaction type to fin sweep is presented in Fig. 21, where a 1-deg sweep change produced a marked difference in shock pattern. The image

corresponding to a fin sweep of −38 deg is an example of a Type II interaction, and the image corresponding to a fin sweep of −39 deg is an example of a Type I interaction. Both of these cases were acquired at a freestream unit Reynolds number of 2×10^6/ft.

Concluding Remarks

A study to examine the effect of fin leading-edge sweep angle on the shock interaction process has been performed in the NASA Langley Research Center 20-Inch Mach 6 Tunnel. The shock interaction was produced by the intersection of a planar incident shock and a bow shock formed around a 0.5-in.-diam cylindrical leading-edge fin. The fin sweep angle was varied from 15 deg swept back to 45 deg swept forward. Heating distributions along the stagnation line of the swept fins subjected to a 16.8-deg (relative to the freestream flow) incident shock were obtained. These distributions were complemented with schlieren photography to illustrate the complex interactions. A finer fin sweep-angle increment was used than in previous three-dimensional studies, with emphasis placed on the forward-swept cases, which potentially produce the highest peak heating augmentations. Also, a significant improvement in the spatial density of the thin-film gauges, critical to the accurate measurement of peak heating values, was accomplished for the present study.

The results indicate that for three-dimensional shock interactions, heating augmentations drastically increase when the leading edge of the fin is swept forward toward the incident shock. Peak heating was maximized when the fin was at $\lambda = -15$ and −25 deg. A Type IV interaction occurred when the fin sweep angle was nearly perpendicular to the incident shock ($\lambda = -15$ deg). This produced a peak heating augmentation on the order of 7 times the baseline value. (If lateral conduction effects could be properly taken into account, the peak heating levels might be more on the order of 10 times the baseline value.) An equally high peak heating value was measured at a fin sweep angle that produced a Type III interaction ($\lambda = -25$ deg). Using the leads as a scale reference in the schlieren images, at least three gauges were within the width of the jet associated with the Type IV cases, which is an indication that the gauge resolution was adequate.

References

[1]Edney, B., "Anomalous Heat Transfer and Pressure Distributions on Blunt Bodies at Hypersonic Speeds in the Presence of an Impinging Shock," Aeronautical Research Inst. of Sweden, Rept. 115, Feb. 1968.

[2]Holden, M., and Kolly, J., "Measurements of Heating in Regions of Shock/Shock Interaction in Hypersonic Flow," AIAA Paper 95-0640, Jan. 1995.

[3]Hackett, C. M., and Calleja, J., "Exploratory Study of Heating Due to a Hypersonic, High-Enthalpy Shock/Shock Interaction," AIAA Paper 95-2216, June 1995.

[4]Carlson, A. B., and Wilmoth, R. G., "Monte Carlo Simulation of a Near-Continuum Shock–Shock Interaction Problem," *Journal of Spacecraft and Rockets*, Vol. 31, No. 1, 1994, pp. 25–30.

[5]Prabhu, R. K., "An Implementation of a Chemical and Thermal Nonequilibrium Flow Solver on Unstructured Meshes and Application to Blunt Bodies," NASA CR 194967, Aug. 1994.

[6]Vemaganti, G. R., "Laminar and Turbulent Flow Computations of Type IV Shock–Shock Interference Aerothermal Loads Using Unstructured Grids," NASA CR 195008, Oct. 1994.

[7]Bushnell, D. M., "Interference Heating on a Swept Cylinder in Region of Intersection with a Wedge at Mach Number 8," NASA TN D-3094, Dec. 1965.

[8]Bushnell, D. M., "Effects of Shock Impingement and Other Factors on Leading-Edge Heat Transfer," NASA TN D-4543, April 1968.

[9]Heirs, R. S., and Loubsky, W. J., "Effects of Shock-Wave Impingement on the Heat Transfer on a Cylindrical Leading Edge," NASA TN D-8859, Feb. 1967.

[10]Keyes, J. W., and Hains, F. D., "Analytical and Experimental Studies of Shock Interference Heating in Hypersonic Flow," NASA TN D-7139, May 1973.

[11]Singh, D. J., Kumar, A., and Tiwari, S. N., "Three-Dimensional Shock–Shock Interactions on the Scramjet Inlet," AIAA Paper 90-0529, Jan. 1990.

[12]Singh, D. J., Kumar, A., and Tiwari, S. N., "Numerical Simulation of Three-Dimensional Shock–Shock Interactions on a Blunt Body," *Computational Fluid Dynamics*, Vol. 1, Gordon and Breach, New York, 1993, pp. 177–196.

[13]Miller, C. G., "Langley Hypersonic Aerodynamic/Aerothermodynamic Testing Capabilities—Present and Future," AIAA Paper 90-1376, June 1990.

[14]Micol, J. R., "Hypersonic Aerodynamic/Aerothermodynamic Testing Capabilities at Langley Research Center: Aerothermodynamic Facilities Complex," AIAA Paper 95-2107, June 1995.

[15]Miller, C. G., "Comparison of Thin-Film Resistance Heat-Transfer Gages with Thin-Skin Transient Calorimeter Gages in Conventional Hypersonic Wind Tunnels," NASA TM 83197, Dec. 1981.

[16]Miller, C. G., Micol, J. R., and Gnoffo, P. A., "Laminar Heat-Transfer Distributions on Biconics at Incidence in Hypersonic–Hypervelocity Flows," NASA TP 2213, 1984.

[17]Hollis, B. R., "User's Manual for the One Dimensional Hypersonic Experimental Aero-Thermodynamic (1DHEAT) Data Reduction Code," NASA CR 4691, Aug. 1995.

[18]Cook, W. J., and Felderman, E. J., "Reduction of Data from Thin-Film Heat-Transfer Gages: A Concise Numerical Technique," *AIAA Journal*, Vol. 4, No. 3, 1966, pp. 561, 562.

[19]Hollis, B. R., and Perkins, J. N., "High-Enthalpy and Perfect Gas Heating Measurements on a Blunt Cone," *Journal of Spacecraft and Rockets*, Vol. 33, No. 5, 1996, pp. 628–634.

[20]Micol, J. R., "Aerothermodynamic Measurement and Prediction for Modified Orbiter at Mach 6 and 10," *Journal of Spacecraft and Rockets*, Vol. 32, No. 5, 1995, pp. 737–748.

B. A. Bhutta
Associate Editor